IMPROVING VAEs' ROBUSTNESS TO ADVERSARIAL ATTACK

Anonymous authors
Paper under double-blind review

ABSTRACT

Variational autoencoders (VAEs) have recently been shown to be vulnerable to adversarial attacks, wherein they are fooled into reconstructing a chosen target image. However, how to defend against such attacks remains an open problem. We make significant advances in addressing this issue by introducing methods for producing adversarially robust VAEs. Namely, we first demonstrate that methods proposed to obtain disentangled latent representations produce VAEs that are more robust to these attacks. However, this robustness comes at the cost of reducing the quality of the reconstructions. We ameliorate this by applying disentangling methods to hierarchical VAEs. The resulting models produce high–fidelity autoencoders that are also adversarially robust. We confirm their capabilities on several different datasets and with current state–of–the–art VAE adversarial attacks, and also show that they increase the robustness of downstream tasks to attack.

1 INTRODUCTION

Variational autoencoders (VAEs) are a powerful approach to learning deep generative models and probabilistic autoencoders (Kingma & Welling, 2014; Rezende et al., 2014). However, previous work has shown that they are vulnerable to adversarial attacks (Tabacof et al., 2016; Gondim-Ribeiro et al., 2018; Kos et al., 2018): an adversary attempts to fool the VAE to produce reconstructions similar to a chosen target by adding distortions to the original input, as shown in Fig 1. This kind of attack can be harmful when the encoder's output is used downstream, as in Xu et al. (2017); Kusner et al. (2017); Theis et al. (2017); Townsend et al. (2019); Ha & Schmidhuber (2018); Higgins et al. (2017b). As VAEs are often themselves used to protect classifiers from adversarial attack (Schott et al., 2019; Ghosh et al., 2019), ensuring VAEs are robust to adversarial attack is an important endeavour.

Despite these vulnerabilities, little progress has been made in the literature on how to ***defend*** VAEs from such attacks. The aim of this paper is to investigate and introduce possible strategies for defence. We seek to defend VAEs in a manner that maintains reconstruction performance. Further, we are also interested in whether methods for defence increase the robustness of downstream tasks using VAEs.

Our first contribution is to show that regularising the variational objective during training can lead to more robust VAEs. Specifically, we leverage ideas from the disentanglement literature (Mathieu et al., 2019) to improve VAEs' robustness by learning simpler and smoother representations that are less vulnerable to attack. In particular, we show that the total correlation (TC) term used into encourage independence between the dimensions of the learned latent representations (Kim & Mnih, 2018; Chen et al., 2018; Esmaeili et al., 2019) also serves as an effective regulariser for learning robust VAEs.

Though a clear improvement over the standard VAE, a severe drawback of this approach is that the gains in robustness are coupled with drops in the reconstruction performance, due to the increased regularisation. Furthermore, we find that the achievable robustness with this approach can be limited (see Fig 1) and thus potentially insufficient for particularly sensitive tasks. To address this, we apply TC–regularisation to *hierarchical* VAEs. By using a richer latent space representation than a standard VAE, the resulting models are not only even more robust to adversarial attacks than single-layer models with TC regularisation, but can also provide reconstructions which are comparable to, and often even better than, the standard (unregularised, single-layer) VAE.

To summarize: We provide insights into what makes VAEs vulnerable to attack and how we might go about defending them. We unearth novel connections between disentanglement and adversarial robustness. We demonstrate that regularised VAEs, trained with an up-weighted total correlation,

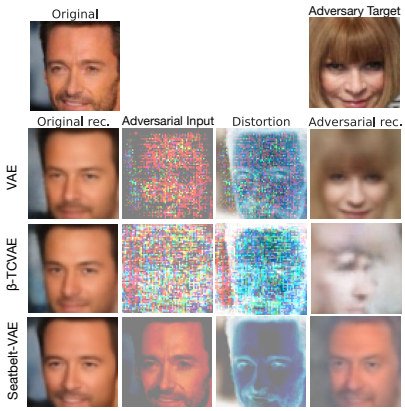

Figure 1: Adversarial attacks on CelebA for different models. Here we start with the image of Hugh Jackman and introduce an adversary that tries to produce reconstructions that look like Anna Wintour. This is done by applying a distortion (third column) to the original image to produce an adversarial input (second column). We can see that the adversarial reconstruction for the Vanilla VAE looks substantially like Wintour, indicating a successful attack. Adding a regularisation term using the β-TCVAE produces an adversarial reconstruction that does not look like Wintour, but it is also far from a successful reconstruction. The hierarchical version of a β-TCVAE (which we call Seatbelt-VAE) is sufficiently hard to attack that the output under attack still looks like Jackman, not Wintour.

are significantly more robust to attacks than vanilla VAEs. Building on this we develop regularised hierarchical VAEs that provide both further robustness to adversarial attack and improved reconstructions. Finally, we show that robustness to adversarial attack also confers increased robustness to downstream tasks.

2 Background: Attacking VAEs

In adversarial attacks, an agent is trying to manipulate the behaviour of some model towards a goal of their choosing, such as fooling a classifier to misclassify an image through adding a small perturbation (Akhtar & Mian, 2018; Gilmer et al., 2018). For many deep learning models, very small changes in the input, imperceptible or unimportant to the human eye, can produce large changes in output.

Attacks on VAEs have been proposed where the adversary looks to apply small input distortions that produce reconstructions close to a target adversarial image (Tabacof et al., 2016; Gondim-Ribeiro et al., 2018; Kos et al., 2018). An example of this is shown in Fig 1, where a standard VAE is successfully attacked to turn Hugh Jackman into Anna Wintour.

The current most effective mode of attack on VAEs is known as a *latent space attack* (Tabacof et al., 2016; Gondim-Ribeiro et al., 2018; Kos et al., 2018). This aims to find a distorted image $\mathbf{x}^* = \mathbf{x} + \mathbf{d}$ such that its posterior $q_\phi(\mathbf{z}|\mathbf{x}^*)$ is close to that of the agent's chosen target image $q_\phi(\mathbf{z}|\mathbf{x}^t)$. This implies that the likelihood $p_\theta(\mathbf{x}^t|\mathbf{z})$ is high given draws from the posterior of the adversarial example. It is particularly important to be robust to this attack if one is concerned with using the encoder network of a VAE as part of a downstream task. For a VAE with a single stochastic layer, the latent-space adversarial objective is (Tabacof et al., 2016; Gondim-Ribeiro et al., 2018)

$$\Delta(\mathbf{x}, \mathbf{d}, \mathbf{x}^t; \lambda) = D_{\mathrm{KL}}(q_\phi(\mathbf{z}|\mathbf{x}+\mathbf{d})||q_\phi(\mathbf{z}|\mathbf{x}^t)) + \lambda||\mathbf{d}||_2, \tag{1}$$

where we are penalising the L_2 norm of $\mathbf{d}$ so as to aim for attacks that change the image less. We can then simply optimise to find a good distortion $\mathbf{d}$.

3 Defending VAEs

Given these approaches to attacking VAEs, the critical question is now how to defend them. This problem was not considered by prior works. To address it, we first need to consider what makes VAEs vulnerable to adversarial attacks. We argue that two key factors dictate whether we can perform a successful attack on a VAE: a) whether we can induce significant changes in the encoding distribution $q_\phi(\mathbf{z}|\mathbf{x})$ through only small changes in the data $\mathbf{x}$, and b) whether we can induce significant changes in the reconstructed images through only small changes to the latents $\mathbf{z}$. The first of these relates to the ***smoothness*** of the encoder mapping, the latter to the smoothness of the decoder mapping.

Consider, for the sake of argument, the case where the encoder–decoder process is almost completely noiseless. Here successful reconstruction places no direct pressure for similar encodings to correspond to similar images: given sufficiently powerful networks very small changes to embeddings $\mathbf{z}$ can imply very large changes to the reconstructed image; there is no ambiguity in the "correct" encoding of a particular datapoint. In essence, we can have lookup–table style behaviour: nearby realisations of $\mathbf{z}$ do not necessarily relate to each other and very different images can have very similar encodings.

This will now be very vulnerable to adversarial attacks: small input changes can lead to large changes in the encoding, and small encoding changes can lead to large changes in the reconstruction. It will also tend to overfit and have gaps in the aggregate posterior, $q_\phi(\mathbf{z}) = \frac{1}{N}\sum_{n=1}^{N} q_\phi(\mathbf{z}|\mathbf{x}_n)$, as each $q_\phi(\mathbf{z}|\mathbf{x}_n)$ will be sharply peaked. These gaps can then be exploited by an adversary.

We postulate two possible ways to avoid this undesirable behaviour. Firstly, we can try and directly regulate the networks used by the encoder and decoder to limit the capacity of the system to have small differences in images induce large differences in latents. Secondly, we can try to regulate the level of noise in the encoding to indirectly force a smoothness in the embedding. Having a noisy encoding creates uncertainty in the latent that gives rise to a particular image, forcing similar latents to correspond to similar images. In other words, we can avoid the aforementioned vulnerabilities by either ensuring our encode–decode process is sufficiently simple, or sufficiently noisy. The fact that the VAE is vulnerable to adversarial attack suggests that its standard setup does not sufficiently encourage either of these to provide an adequate defence. Introducing additional regularisation to enforce simplicity or noisiness thus provides an intriguing prospect for defending VAEs.

Though, in principle, direct regularisation of the networks (e.g. weight decay) might be a viable defence in some scenarios, we will instead focus on indirect regularisation approaches as discussed in the next section. The reason for this is that controlling the macroscopic behaviour of the networks through low-level regularisations can be difficult to control and, in particular, difficult to calibrate.

3.1 Disentanglement and Robustness

Recent research into disentangling VAEs (Higgins et al., 2017a; Siddharth et al., 2017; Kim & Mnih, 2018; Chen et al., 2018; Esmaeili et al., 2019; Mathieu et al., 2019) and the information bottleneck (Alemi et al., 2017; 2018) has looked to regularise the ELBO with the hope of providing more interpretable or simpler embeddings. Disentangling can be difficult to achieve in practice, and often requires precisely choosing the hyperparameters of the model *and* of the weighting of the added regularisation term (Locatello et al., 2019; Mathieu et al., 2019; Rolinek et al., 2019). Nevertheless, these approaches hint at an interesting link, raising the question: *can we use methods initially proposed to encourage disentanglement to encourage robustness*?

Of particular relevance, Mathieu et al. (2019) introduce the notion of ***overlap*** in the embedding of a VAE and show how controlling it is critical to achieving smooth and meaningful latent representations. Overlap encapsulates both the level of uncertainty in the encoding process and also a locality of this uncertainty: to learn a smooth representation we not only need our encoder distribution to have an appropriate entropy, we also want the different possible encodings to be similar to each other, rather than spread out. They further show that the success of many methods for disentanglement, and in particular the β-VAE (Higgins et al., 2017a; Alemi et al., 2017), work by controlling overlap.

Regularising for Robustness There are a number of different disentanglement methods that one might consider using to train robust VAEs. Perhaps the simplest would be to use a β-VAE (Higgins et al., 2017a), wherein we up-weight the D_{KL} term in the VAE's ELBO by a factor $\beta \geq 1$. However, as mentioned previously the β-VAE only provides disentanglement at the expense of substantial reductions in reconstruction quality as the data likelihood term has, in effect, been down-weighted (Kim & Mnih, 2018; Chen et al., 2018; Mathieu et al., 2019). Furthermore, the level of disentanglement it can achieve is lesser than more recent methods (Kim & Mnih, 2018; Chen et al., 2018).

Because of these shortfalls, we instead propose to regularise through penalisation of a total correlation (TC) term (Kim & Mnih, 2018; Chen et al., 2018). As discussed in Section A.1, this looks to directly force independence across the different latent dimensions in aggregate posterior $q_\phi(\mathbf{z})$, such that the aggregate posterior factorises across dimensions. This approach has been shown to have a smaller deleterious effect on reconstruction quality than found in β-VAEs (Chen et al., 2018). As seen in Fig 2 this method also gives greater overlap by increasing posterior variance. To summarise, the greater overlap and the lesser degradation of reconstruction quality induced by β-TCVAE make them highly suitable for our purposes.

3.2 Adversarial Attacks on TC-Penalised VAEs

We now consider attacking these TC-penalised VAEs and demonstrate one of the key contributions of the paper: that empirically this form of regularisation makes adversarial attacks on VAEs harder to carry out. To do this, we first train them under the β-TCVAE objective (i.e. Eq (14)), jointly

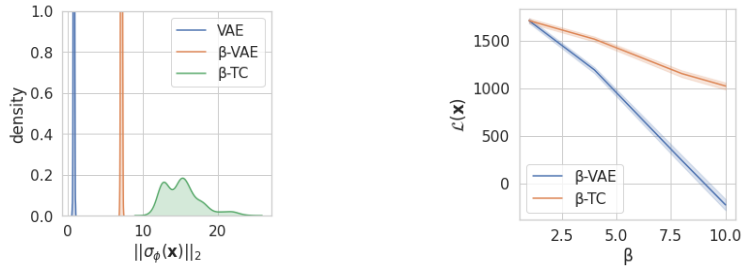

Figure 2: [Left] density plot of $||\boldsymbol{\sigma}_\phi(\mathbf{x})||_2$ for a VAE, a β-VAE and a β-TCVAE each trained on CelebA, $\beta = 10$. The β-VAE's posterior variance saturates, while the β-TCVAE's does not and as such is able to induce more overlap. [Right] the ELBO for both under varying β values. Clearly the model quality degrades to a lesser degree for the TC-penalised models under increasing β.

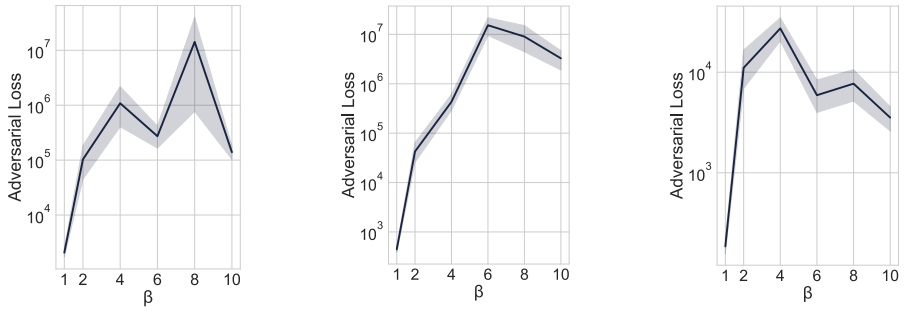

(a) dSprites (b) Chairs (c) 3D Faces

Figure 3: Attacker's achieved loss Δ (i.e. Eq (1)) for β-TCVAE for different β values and datasets. Higher loss indicates more robustness. Shading corresponds to the 95% CI produced by attacking 20 images for each combination of $d_{\mathbf{z}} = \{4, 8, 16, 32, 64, 128\}$ and taking 50 geometrically distributed values of λ between 2^{-20} and 2^{20} (giving 1000 total trials). Note that the loss axis is logarithmic. $\beta > 1$ clearly induces a much larger loss for the adversary relative to $\beta = 1$ for all datasets.

optimising θ, ϕ for a given β. Once trained, we then attack the models using the methods outlined in Section 2, finding an input distortion $\mathbf{d}$ that minimises the attack loss Δ as per Eq (1).

One possible metric for how successfully such attacks have been is the achieved value reached of the attack loss Δ. If the latent space distributions for the original input and for the distorted input match exactly for a small distortion, then Δ too is small and the model has been successfully fooled: reconstructions from samples from the attacked posterior would be indistinguishable from those from the target posterior. Meanwhile, the larger the converged value of the attack loss the less similar these distributions are and the more different the reconstructed image is to the adversarial target image.

We carry our these attacks for dSprites (Matthey et al., 2017), Chairs (Aubry et al., 2014) and 3D faces (Paysan et al., 2009), for a range of β and λ values. We pick values of λ following standard methodology (Tabacof et al., 2016; Gondim-Ribeiro et al., 2018), and use L-BFGS-B for gradient descent (Byrd et al., 1995). We also tried varying the dimensionality of the latent space of the model, $d_{\mathbf{z}}$, but found it had little effect on the effectiveness of the attack.

In Fig 3 we show the effect on the attack loss Δ from varying β, averaged over different original input-target pairs and values of $d_{\mathbf{z}}$. Note that the plot is logarithmic in the loss. We see a clear pattern for each dataset that the loss values reached by the adversary increases as we increase β from the standard VAE (i.e. $\beta = 1$). This analysis is also borne out by visual inspection of the effectiveness of these attacks, for example as shown in Fig 1. We will return to give further experimental results in Section 5. An interesting point of note in Fig 3 is that in many cases the adversarial loss starts to decrease if β is set too large: as β increases there is less pressure in the objective to produce good reconstructions.

4 HIERARCHICAL TC–PENALISED VAES

We are now armed with the fact that penalising the TC in the ELBO induces robustness in VAEs. However, TC-penalisation in single layer VAEs comes at the expense of model reconstruction quality (Chen et al., 2018). Our aim is to develop a model that is robust to adversarial attack while mitigating this trade-off between robustness and sample quality. To achieve this, we now consider instead using hierarchical VAEs (Rezende et al., 2014; Sønderby et al., 2016; Kingma et al., 2016; Zhao et al., 2017; Maaløe et al., 2019). These are known for their superior modelling capabilities and more accurate reconstructions. As these gains stem from using more complex hierarchical latent spaces, rather than less noisy encoders, this suggests they may be able to produce better reconstructions and generative capabilities, while also remaining robust to adversarial attacks when appropriately regularised.

The simplest hierarchical extension of conditional stochastic variables in the generative model is the Deep Latent Gaussian Model (DLGM) of Rezende et al. (2014). Here the forward model factorises as a chain, $p_\theta(\mathbf{x}, \vec{\mathbf{z}}) = p_\theta(\mathbf{x}|\mathbf{z}^1) \prod_{i=1}^{L-1} p_\theta(\mathbf{z}^i|\mathbf{z}^{i+1}) p(\mathbf{z}^L)$, where each $p_\theta(\mathbf{z}^i|\mathbf{z}^{i+1})$ is a Gaussian distribution with mean and variance parameterised by deep nets, while $p(\mathbf{z}^L)$ is an isotropic Gaussian. Unfortunately, we found that naively applying TC-correlation penalisation to DLGM-style VAEs did not confer the improved robustness we observed in single layer VAEs. We postulate that this observed weakness is inherent to the structure of chain factorisation in the generative model: this means that the data-likelihood depends solely on $\mathbf{z}^1$, the bottom-most latent variable, and attackers only need to manipulate $\mathbf{z}^1$ to produce a successful attack.

To account for this, we instead use a generative model in which the likelihood $p_\theta(\mathbf{x}|\vec{\mathbf{z}})$ depends on *all* the latent variables in the chain $\vec{\mathbf{z}}$, rather than just the bottom layer $\mathbf{z}^1$, as has been done in Kingma et al. (2016); Maaløe et al. (2019). This leads to the following factorisation of the generative structure:

$$p_\theta(\mathbf{x}, \vec{\mathbf{z}}) = p_\theta(\mathbf{x}|\vec{\mathbf{z}}) \prod_{i=1}^{L-1} p_\theta(\mathbf{z}^i|\mathbf{z}^{i+1}) p(\mathbf{z}^L). \tag{2}$$

To construct the ELBO, we must further introduce an inference network $q_\phi(\vec{\mathbf{z}}|\mathbf{x})$. On the basis of simplicity and that it produces effective empirical performance, we use the factorisation:

$$q_\phi(\vec{\mathbf{z}}|\mathbf{x}) = q_\phi(\mathbf{z}^1|\mathbf{x}) \prod_{i=1}^{L-1} q_\phi(\mathbf{z}^{i+1}|\mathbf{z}^i, \mathbf{x}), \tag{3}$$

where each conditional distribution $q_\phi(\mathbf{z}^{i+1}|\mathbf{z}^i, \mathbf{x})$ takes the form of a Gaussian. Again, marginalising out intermediate $\mathbf{z}^i$ layers, $q_\phi(\mathbf{z}^L|\mathbf{x})$ is a non-Gaussian, highly flexible, distribution. To defend this model against adversarial attack, we apply TC regularisation term as per the last section. We refer to the resulting models as Seatbelt-VAEs. We obtain a decomposition of the ELBO for this model, revealing the existence of a TC term for the top-most layer (see Appendix B for proof).

Theorem 1. *The Evidence Lower Bound, for a hierarchical VAE with forward model as in Eq* (2) *and amortised variational posterior as in Eq* (3)*, can be decomposed to reveal the total correlation (see Definition A.1), of the aggregate posterior of the top-most layer of latent variables:*

$$\mathcal{L}(\theta, \phi; \mathcal{D}) = \mathbb{E}_{q(\vec{\mathbf{z}}, \mathbf{x})} \log p_\theta(\mathbf{x}|\vec{\mathbf{z}}) + \textcircled{R} + \textcircled{S_a} + \textcircled{S_b} + D_{\mathrm{KL}}\Big(q(\mathbf{z}^L) || \prod_j q(z_j^L)\Big), \tag{4}$$

where the last term is the required TC term, and, using j to index over the coordinates in $\mathbf{z}^L$,

$$\textcircled{R} = \int \mathrm{d}\mathbf{x} \prod_{i=1}^{L} (\mathrm{d}\mathbf{z}^i) q_\phi(\vec{\mathbf{z}}|\mathbf{x}) q(\mathbf{x}) \log \frac{\prod_{k=1}^{L-1} p_\theta(\mathbf{z}^k|\mathbf{z}^{k+1})}{q_\phi(\mathbf{z}^1|\mathbf{x}) \prod_{m=1}^{L-2} q_\phi(\mathbf{z}^{m+1}|\mathbf{z}^m, \mathbf{x})} \tag{5}$$

$$\textcircled{S_a} = -\mathbb{E}_{q_\phi(\mathbf{z}^{L-1})} D_{\mathrm{KL}}(q_\phi(\mathbf{z}^L, \mathbf{x}|\mathbf{z}^{L-1}) || q_\phi(\mathbf{z}^L) q(\mathbf{x})) \tag{6}$$

$$\textcircled{S_b} = -\sum_j D_{\mathrm{KL}}(q_\phi(\mathbf{z}_j^L) || p(\mathbf{z}_j^L)). \tag{7}$$

In other words, following the Factor and β-TCVAEs, we up-weight the TC term for $\mathbf{z}^L$. We can upweight this term then recombine the decomposed parts of the ELBO, to give us the following compact form of this objective.

Definition 1. *A Seatbelt-VAE is a hierarchical VAE with forward model as in Eq* (2) *and amortised variational posterior as in Eq* (3)*, trained wrt its parameters θ, ϕ to maximise the objective:*

$$\mathcal{L}^{\mathrm{Seatbelt}}(\theta, \phi; \beta, \mathcal{D}) := \mathbb{E}_{q_\phi(\vec{\mathbf{z}}, \mathbf{x})} \left[\log \frac{p_\theta(\mathbf{x}, \vec{\mathbf{z}})}{q_\phi(\vec{\mathbf{z}}|\mathbf{x})}\right] - (\beta - 1) D_{\mathrm{KL}}\Big(q(\mathbf{z}^L) || \prod_j q(z_j^L)\Big). \tag{8}$$

We see that, when $L = 1$, a Seatbelt-VAE reduces to a β-TCVAE. We use the $\beta = 1$ case as a baseline in our experiments as it corresponds to a Vanilla VAE for $L = 1$ and for $L > 1, \beta = 1$ it produces a hierarchical model with a likelihood function conditioned on all latents.

As with the β-TCVAE, training $\mathcal{L}^{\text{Seatbelt}}_{\theta,\phi;\beta,\mathcal{D}}$ using stochastic gradient ascent with minibatches of the data is complicated by the presence of aggregate posteriors $q_\phi(\mathbf{z})$ which depend on the entire dataset. To deal with this, Appendix C we derive a minibatch estimator for TC-penalised hierarchical VAEs, building off that used for β-TCVAEs (Chen et al., 2018). We note that, as in (Chen et al., 2018), large batch sizes are generally required to provide accurate TC estimates.

Attacking Hierarchical TC–Penalised VAEs In the above hierarchical model the likelihood over data is conditioned on all layers, so manipulations to any layer have the potential to be significant. We focus on simultaneously attacking all layers, noting that, as shown in Appendix D, this is more effective that just targeting the top or base layers individually. Hence our adversarial objective for Seatbelt-VAEs is the following generalisation of that introduced in Tabacof et al. (2016); Gondim-Ribeiro et al. (2018), to attack all the layers at the same time:

$$\Delta^{\text{Seatbelt}}(\mathbf{x}, \mathbf{d}, \mathbf{x}^t; \lambda) = \lambda||\mathbf{d}||_2 + \sum\nolimits_{i=1}^{L} D_{\text{KL}}(q_\phi(\mathbf{z}^i|\mathbf{x}+\mathbf{d})||q_\phi(\mathbf{z}^i|\mathbf{x}^t)). \tag{9}$$

5 Experiments

Expanding on the brief experiments in Section 3.2, we perform a battery of adversarial attacks on each of the introduced models. We evaluate the effectiveness attack in three ways. First, like Fig 1, we can plot the attacks themselves, to see how effective these attacks are in fooling us. Secondly, we can measure the adversary's loss under the attack objective above. Thirdly, we give the negative adversarial likelihood of the target image $\mathbf{x}^t$ given an attacked latent representation $\mathbf{z}^*$. Larger, more positive values of $-\log p_\theta(\mathbf{x}^t|\mathbf{z}^*)$ correspond to less successful attacks as they correspond to large distances between the target and the adversarial reconstruction. Highly negative values of this correspond to successful attacks as they correspond to a small distance between the adversarial target and the reconstruction. We also measure reconstruction quality of these models, as a function of degree of regularisation. Finally, we also measure how downstream tasks that use output of these models perform under attack. We train two sets of classifiers, on the reconstructions and on the latent representations, and see how robust classification performance is when the upstream VAE is attacked.

We demonstrate that hierarchical TC–Penalised VAEs (Seatbelt-VAEs) confer superior robustness to β-TCVAEs and standard VAEs, while preserving the ability to reconstruct inputs effectively. Through this, we demonstrate that they are a powerful tool for learning robust deep generative models.

Following previous work (Tabacof et al., 2016; Gondim-Ribeiro et al., 2018) we randomly sample 10 input-target pairs for each dataset and for each image pair we consider 50 different values of λ geometrically-distributed from 2^{-20} to 2^{20}. Thus each model undergoes 500 attacks for each attack mode. As before, we used L-BFGS-B for gradient descent (Byrd et al., 1995). We perform these experiments on Chairs (Aubry et al., 2014), 3D faces (Paysan et al., 2009), and CelebA (Liu et al., 2015). Details of neural network architectures and training are given in Appendix G.

5.1 Visual Appraisal of Attacks

We first visually appraise the effectiveness of attacks on vanilla VAEs, β-TCVAEs, and Seatbelt-VAEs. As mentioned in Section 1, Fig 1 shows the results of latent space attacks on three models trained on CelebA. It is apparent that the β-TCVAE provides additional resilience to the attacks compared with the standard VAE. Furthermore, this figure shows that Seatbelt-VAEs are sufficiently robust to almost completely thwart the adversary: its adversarial construction still resembles the original input. Moreover, this was achieved while also producing a clearer non–adversarial reconstruction. One might expect that attacks targeting a single generative factor underpinning the data would be easier for the attacker. However, we find that these models protect effectively against this as well. For example, see Fig 4 for plots showing an attacker attempting to rotate a dSprites heart.

5.2 Quantitative Analysis of Robustness

Having ascertained perceptually that Seatbelt-VAEs offers the strongest protection to adversarial attack, we now demonstrate this quantitatively. Fig 5 shows $-\log p_\theta(\mathbf{x}^t|\mathbf{z}^*)$ and Δ over a range of datasets and βs for Seatbelt-VAEs ($L = 4$) and β-TCVAEs. It demonstrates that the combination

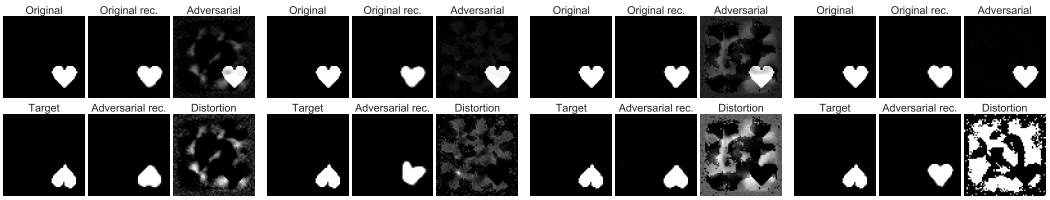

(a) β-TCVAE, β=1 (b) β-TCVAE, β=2 (c) SB-VAE, β=1 (d) SB-VAE, $\beta = 2$

Figure 4: Latent space attacks *only on rotation* of a heart-shaped dSprite for β-TCVAEs ($d_{\mathbf{z}} = 64$) and Seatbelt-VAEs ($L = 2$) for $\beta = \{1, 2\}$. The attacks are conducted by applying a distortion (third column of each image) to the original image (top first column) to produce an adversarial input (bottom second column of each image) to try to cause the output of the target image (bottom first column). Here we show the most successful adversarial distortion in terms of adversarial loss for each model. It is apparent that Seatbelt-VAEs are the most resilient to attack.

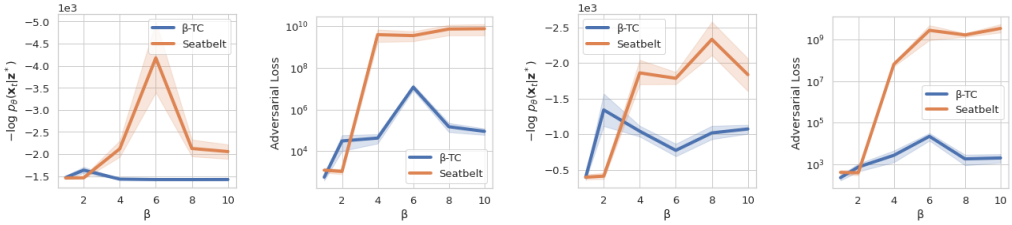

(a) -log $p_\theta(\mathbf{x}^t|\mathbf{z}^*)$ Faces (b) Δ Faces (c) -log $p_\theta(\mathbf{x}^t|\mathbf{z}^*)$ Chairs (d) Δ Chairs

Figure 5: Plots showing the robustness of Seatbelt-VAEs (L=4) and β-TCVAEs models for different values of β. Note that the β-TCVAE with $\beta = 1$ corresponds to a vanilla VAE and that $L > 1$ $\beta = 1$ models correspond to hierarchical baselines. We show the negative adversarial likelihood of a target image $\mathbf{x}^t$ given an attacked latent representation $\mathbf{z}^*$ for Chairs (a) and 3D Faces (b) respectively. Larger values of $-\log p_\theta(\mathbf{x}^t|\mathbf{z}^*)$ mean less successful adversarial attacks. We also show the adversarial loss Δ in subfigures (b) and (d), which have a logarithmic axis. Shading in results corresponds to the 95% CI over variation for 10 images for each combination of $d_{\mathbf{z}} = \{4, 8, 16, 32, 64, 128\}$ and λ taking 50 geometrically distributed values between 2^{-20} and 2^{20}.

of depth and high TC-penalisation offers the best protection to adversarial attacks and that the hierarchical extension confers much greater protection to adversarial attack than a single layer β-TCVAE. As we go to the largest values of β for both Chairs and 3D Faces, adversarial loss Δ grows by a factor of $\approx 10^7$ and $-\log p_\theta(\mathbf{x}^t|\mathbf{z}^*)$ doubles for Seatbelt-VAE. β-TCVAEs do not experience such a large uptick in adversarial loss and negative adversarial likelihood. These results show that the hierarchical approach can offer very strong protection from the adversarial attacks studied.

See Appendix D for plots detailing these metrics for a range of L values. In Appendix E we also calculate the L_2 distance between target images and adversarial outputs and show that the loss of effectiveness of adversarial attacks is not due to the degradation of reconstruction quality from increasing β. There we also include results for "output" attacks: here the attacker directly tries to reduce the L_2 distance between the reconstructed output and the target image. In line with previous work we find this to be generally less effective as an attack mode (Gondim-Ribeiro et al., 2018; Kos et al., 2018). Again, TC-penalised models outperformed standard VAEs.

We also test VAE robustness to random noise. We noise the inputs and evaluate the model's ability to reconstruct the original datapoint. Through this we are evaluating their ability to denoise. See Appendix F for an illustration of the denoising properties of TC-penalised models. It is plausible that the ability of these models' to denoise is linked to their robustness to attacks.

5.3 ELBO and Reconstruction Quality

Though Seatbelt–VAEs offer better protection to adversarial attack than β-TCVAEs, we also motivate their utility by way of their reconstruction quality. In Fig 6 we plot the final ELBO of the two TC-penalised models, but calculated *without* the additional β penalisation that was applied during training. We further show the effect of depth and TC-penalisation on CelebA reconstructions. These

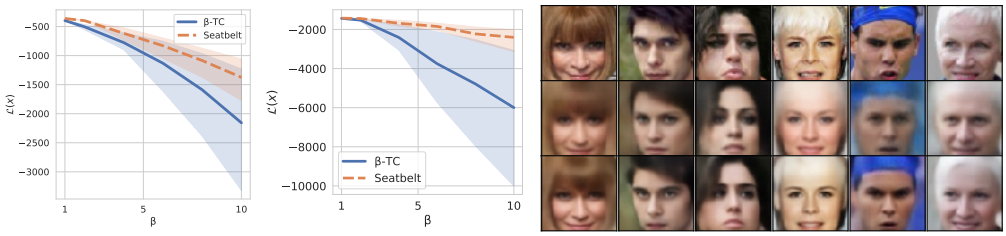

(a) Chairs ELBO (b) 3D Faces ELBO (c) Reconstructions

Figure 6: Effect of varying β on the reconstructions of TC-penalised models. In sub-figures (a) and (b) we plot the final ELBO of TC-penalised models trained on the Chairs and 3D faces, calculated *without* the β penalisation applied during training. Shading gives the 95% CI over variation due to variation of $d_{\mathbf{z}} = \{32, 64, 128\}$ for β-TCVAE and also $L = \{2, 3, 4, 5\}$ for Seatbelt. As β increases $\mathcal{L}$ degrades more slowly for Seatbelt-VAE, relative to β-TCVAE, (c) serves as a visual confirmation of these results. The top row shows CelebA input data. The bottom row, the reconstructions from a Seatbelt-VAE with $L = 4$ and $\beta = 20$, clearly maintains facial identity better than those from a β-TCVAE, the middle row: many of the individuals' finer facial features lost by the β-TCVAE are maintained by the Seatbelt-VAE.

plots show that Seatbelt-VAEs' reconstructions are more resilient to increasing β than β-TCVAEs', both visually as well as measurably.

5.4 Protection to Downstream Tasks

Table 1: Robustness of downstream classification tasks under adversarial attack. We consider classifiers trained either on the reconstructed image (denoted $p(y|\tilde{\mathbf{x}})$) or on the latent representations ($p(y|\mathbf{z})$). We show accuracy when the model is attacked, resulting in perturbed embeddings $\mathbf{z}^*$ and reconstructions ($\tilde{\mathbf{x}}^*$). Parentheses show the drop in accuracy resulting from the attack – the smaller the drop in magnitude the better

		Accuracy by Model		
Dataset	Task	VAE	β–TCVAE	Seatbelt–VAE
SVHN	$p(y\|\tilde{\mathbf{x}})$	0.17 (-0.35)	0.22 (-0.29)	**0.35** (**-0.15**)
	$p(y\|\mathbf{z})$	0.15 (-0.57)	0.46 (-0.23)	**0.57** (**-0.21**)
CIFAR10	$p(y\|\tilde{\mathbf{x}})$	0.17 (-0.32)	0.25 (-0.21)	**0.38** (**-0.09**)
	$p(y\|\mathbf{z})$	0.16 (-0.41)	0.26 (-0.23)	**0.39** (**-0.09**)

Finally, we consider the protection that Seatbelt-VAEs might provide to downstream tasks, noting that VAEs are often used as subcomponents in larger ML systems (Higgins et al., 2017b), or as a mechanism to protect another model from attack (Schott et al., 2019; Ghosh et al., 2019). Table 1 shows results for classification tasks based on using 2-layer MLPs trained on either the embeddings or the reconstructions. Specifically, it shows the drop in accuracy caused by an adversary that picks a target with a different label and attacks the VAEs' embedding using the attack objective with $\lambda = 1$. We see that Seatbelt–VAEs produced significantly better accuracies under these attacks.

6 Conclusion

We have shown that VAEs can be rendered more robust to adversarial attacks by regularising the evidence lower bound. This increase in robustness can be strengthened by extending these regularisation methods to hierarchical VAEs, forming Seatbelt-VAEs, which uses a generative structure where the likelihood makes use of all the latent variables. Designing robust VAEs is becoming pressing as they are increasingly deployed as subcomponents in larger pipelines. As we have shown, methods typically used for disentangling, motivated by their ability to provide interpretable representations, also confer robustness. Studying the beneficial effects of these methods is starting to come to the fore of VAE research (Kumar & Poole, 2020). We hope this work sparks further interest in the interplay between disentangling, regularisation, and model robustness.

REFERENCES

Naveed Akhtar and Ajmal Mian. Threat of Adversarial Attacks on Deep Learning in Computer Vision: A Survey. *IEEE Access*, 6:14410–14430, 2018. ISSN 21693536. doi: 10.1109/ACCESS.2018.2807385.

Alexander A Alemi, Ian Fischer, Joshua V Dillon, and Kevin Murphy. Deep Variational Information Bottleneck. In *ICLR*, 2017. ISBN 1612.00410v5.

Alexander A Alemi, Ben Poole, Ian Fischer, Joshua V Dillon, Rif A Saurous, and Kevin Murphy. Fixing a Broken ELBO. In *ICML*, 2018.

Mathieu Aubry, Daniel Maturana, Alexei A Efros, Bryan C Russell, and Josef Sivic. Seeing 3D chairs: Exemplar part-based 2D-3D alignment using a large dataset of CAD models. In *Proceedings of the IEEE Computer Society Conference on Computer Vision and Pattern Recognition*, pp. 3762–3769, 2014. ISBN 9781479951178. doi: 10.1109/CVPR.2014.487.

Anthony J Bell and Terrence J Sejnowski. An information-maximisation approach to blind separation and blind deconvolution. *Neural Computation*, 7(6):1004–1034, 1995.

Yoshua Bengio, Aaron Courville, and Pascal Vincent. Representation learning: A review and new perspectives. *IEEE Transactions on Pattern Analysis and Machine Intelligence*, 35(8):1798–1828, 2013. ISSN 01628828. doi: 10.1109/TPAMI.2013.50. URL `http://www.image-net.org/challenges/LSVRC/2012/results.html`.

Yuri Burda, Roger Grosse, and Ruslan Salakhutdinov. Importance Weighted Autoencoders. In *ICLR*, 2016. URL `https://arxiv.org/pdf/1509.00519.pdf`.

Christopher P Burgess, Irina Higgins, Arka Pal, Loic Matthey, Nick Watters, Guillaume Desjardins, Alexander Lerchner, and Deepmind London. Understanding disentangling in beta-VAE. In *NeurIPS*, 2017.

Richard H Byrd, Peihuang Lu, Jorge Nocedal, and Ciyou Zhu. A Limited Memory Algorithm for Bound Constrained Optimization. *SIAM J. Sci. Comput.*, 16(5):1190–1208, 9 1995. ISSN 1064-8275. doi: 10.1137/0916069.

Ricky T Q Chen, Xuechen Li, Roger Grosse, and David Duvenaud. Isolating Sources of Disentanglement in Variational Autoencoders. In *NeurIPS*, 2018.

Babak Esmaeili, Hao Wu, Sarthak Jain, Alican Bozkurt, N Siddharth, Brooks Paige, Dana H Brooks, Jennifer Dy, and Jan-Willem van de Meent. Structured Disentangled Representations. In *AISTATS*, 2019.

Partha Ghosh, Arpan Losalka, and Michael J Black. Resisting Adversarial Attacks Using Gaussian Mixture Variational Autoencoders. In *AAAI*, 2019.

Justin Gilmer, Ryan P Adams, Ian Goodfellow, David Andersen, and George E Dahl. Motivating the Rules of the Game for Adversarial Example Research. *CoRR*, 2018.

George Gondim-Ribeiro, Pedro Tabacof, and Eduardo Valle. Adversarial Attacks on Variational Autoencoders. *CoRR*, 2018.

David Ha and Jürgen Schmidhuber. World Models. In *NeurIPS*, 2018. doi: 10.5281/zenodo.1207631.

Irina Higgins, Loic Matthey, Arka Pal, Christopher Burgess, Xavier Glorot, Matthew Botvinick, Shakir Mohamed, and Alexander Lerchner. β-VAE: Learning Basic Visual Concepts with a Constrained Variational Framework. In *ICLR*, 2017a. doi: 10.1177/1078087408328050.

Irina Higgins, Arka Pal, Andrei Rusu, Loic Matthey, Christopher Burgess, Alexander Pritzel, Matthew Botvinick, Charles Blundell, and Alexander Lerchner. DARLA: Improving Zero-Shot Transfer in Reinforcement Learning. In *ICML*, 2017b.

Matthew D Hoffman and Matthew J Johnson. ELBO surgery: yet another way to carve up the variational evidence lower bound. In *NeurIPS*, 2016.

Ilyes Khemakhem, Diederik P Kingma, Ricardo Pio Monti, and Aapo Hyvärinen. Variational Autoencoders and Nonlinear ICA: A Unifying Framework. In *AISTATS*, 2020.

Hyunjik Kim and Andriy Mnih. Disentangling by Factorising. In *NeurIPS*, 2018.

Diederik P Kingma and Jimmy Lei Ba. Adam: A Method for Stochastic Optimisation. In *ICLR*, 2015. URL https://arxiv.org/pdf/1412.6980.pdf.

Diederik P Kingma and Max Welling. Auto-encoding Variational Bayes. In *ICLR*, 2014.

Diederik P Kingma, Tim Salimans, Rafal Jozefowicz, Xi Chen, Ilya Sutskever, and Max Welling. Improving Variational Inference with Inverse Autoregressive Flow. In *NeurIPS*, 2016. URL https://arxiv.org/pdf/1606.04934.pdf.

J Kos, I Fischer, and D Song. Adversarial Examples for Generative Models. In *IEEE Security and Privacy Workshops*, pp. 36–42, 5 2018. doi: 10.1109/SPW.2018.00014.

Tejas D Kulkarni, Will Whitney, Pushmeet Kohli, and Joshua B Tenenbaum. Deep Convolutional Inverse Graphics Network. In *NeurIPS*, 2015. doi: 10.1063/1.4914407. URL https://arxiv.org/pdf/1503.03167.pdfhttp://arxiv.org/abs/1503.03167.

Abhishek Kumar and Ben Poole. On Implicit Regularization in β-VAE. In *ICML*, 2020.

Matt J Kusner, Brooks Paige, and José Miguel Hernández-Lobato. Grammar Variational Autoencoder. In *ICML*, 2017.

Ziwei Liu, Ping Luo, Xiaogang Wang, and Xiaoou Tang. Deep Learning Face Attributes in the Wild. In *Proceedings of International Conference on Computer Vision (ICCV)*, 2015.

Francesco Locatello, Stefan Bauer, Mario Lucie, Gunnar Rätsch, Sylvain Gelly, Bernhard Schölkopf, and Olivier Bachem. Challenging common assumptions in the unsupervised learning of disentangled representations. In *ICML*, volume 2019-June, 2019. ISBN 9781510886988. URL https://github.com/google-research/.

Lars Maaløe, Marco Fraccaro, Valentin Liévin, and Ole Winther. BIVA: A Very Deep Hierarchy of Latent Variables for Generative Modeling. In *NeurIPS*, 2019.

Alireza Makhzani, Jonathon Shlens, Navdeep Jaitly, Ian Goodfellow, and Brendan Frey. Adversarial Autoencoders. In *ICLR*, 2016. ISBN 0928-4931. doi: 10.1016/j.msec.2012.07.027. URL https://arxiv.org/pdf/1511.05644.pdf.

Emile Mathieu, Tom Rainforth, N. Siddharth, and Yee Whye Teh. Disentangling Disentanglement in Variational Autoencoders. In *ICML*, 2019.

Loic Matthey, Irina Higgins, Demis Hassabis, and Alexander Lerchner. dSprites: Disentanglement testing Sprites dataset, 2017.

Pascal Paysan, Reinhard Knothe, Brian Amberg, Sami Romdhani, and Thomas Vetter. A 3D face model for pose and illumination invariant face recognition. In *6th IEEE International Conference on Advanced Video and Signal Based Surveillance, AVSS 2009*, pp. 296–301, 2009. ISBN 9780769537184. doi: 10.1109/AVSS.2009.58.

Tom Rainforth, Robert Cornish, Hongseok Yang, Andrew Warrington, and Frank Wood. On nesting Monte Carlo estimators. In *ICML*, 2018. ISBN 9781510867963.

Danilo Jimenez Rezende, Shakir Mohamed, and Daan Wierstra. Stochastic Backpropagation and Approximate Inference in Deep Generative Models. In *ICML*, 2014.

Michal Rolinek, Dominik Zietlow, and Georg Martius. Variational autoencoders pursue pca directions (by accident). In *Proceedings of the IEEE Computer Society Conference on Computer Vision and Pattern Recognition*, volume 2019-June, pp. 12398–12407, 2019. ISBN 9781728132938. doi: 10.1109/CVPR.2019.01269.

Lukas Schott, Jonas Rauber, Matthias Bethge, and Wieland Brendel. Toward the First Adversarially Robust Neural Network Model on MNIST. In *ICLR*, 2019.

N Siddharth, Brooks Paige, Jan Willem Van De Meent, Alban Desmaison, Noah D Goodman, Pushmeet Kohli, Frank Wood, and Philip H.S. Torr. Learning disentangled representations with semi-supervised deep generative models. In *NeurIPS*, 2017.

Casper Kaae Sønderby, Tapani Raiko, Lars Maaløe, Søren Kaae Sønderby, and Ole Winther. Ladder Variational Autoencoders. In *NeurIPS*, 2016.

Pedro Tabacof, Julia Tavares, and Eduardo Valle. Adversarial Images for Variational Autoencoders. In *NIPS Workshop on Adversarial Training*, 2016.

Lucas Theis, Wenzhe Shi, Andrew Cunningham, and Ferenc Huszár. Lossy Image Compression with Compressive Autoencoders. In *ICLR*, 2017.

James Townsend, Tom Bird, and David Barber. Practical Lossless Compression with Latent Variables using Bits Back Coding. In *ICLR*, 2019.

Satosi Watanabe. Information Theoretical Analysis of Multivariate Correlation. *IBM Journal of Research and Development*, 4(1):66–82, 1960. ISSN 0018-8646. doi: 10.1147/rd.41.0066.

Weidi Xu, Haoze Sun, Chao Deng, and Ying Tan. Variational Autoencoder for Semi-supervised Text Classification. In *AAAI*, pp. 3358–3364, 2017. ISBN 9781450329569. doi: 10.1051/0004-6361/201527329.

Shengjia Zhao, Jiaming Song, and Stefano Ermon. Learning Hierarchical Features from Generative Models. In *ICML*, 2017.

A VARIATIONAL AUTOENCODERS

Variational autoencoders (VAEs) are a variety of generative model suitable for high-dimensional data like images (Kingma & Welling, 2014; Rezende et al., 2014). They introduce a joint distribution over data $\mathbf{x}$ and latent variables $\mathbf{z}$: $p_\theta(\mathbf{x}, \mathbf{z}) = p_\theta(\mathbf{x}|\mathbf{z})p(\mathbf{z})$, where $p_\theta(\mathbf{x}|\mathbf{z})$ is an appropriate distribution given the form of the data, the parameters of which are represented by deep nets with parameters θ, and $p(\mathbf{z}) = \mathcal{N}(0, \mathcal{I})$ is a common choice for the prior. As exact inference is intractable, one performs amortised stochastic variational inference by introducing an inference network for the latent variables, $q_\phi(\mathbf{z}|\mathbf{x})$, which often also takes the form of a Gaussian, $\mathcal{N}(\mathbf{z}|\mu_\phi(\mathbf{x}), \Sigma_\phi(\mathbf{x}))$. We can then perform gradient ascent, with respect to both θ and ϕ, on the evidence lower bound (ELBO)

$$\mathcal{L}(\mathbf{x}) = \mathbb{E}_{q_\phi(\mathbf{z}|\mathbf{x})}\left[\log p_\theta(\mathbf{x}|\mathbf{z})\right] - D_{\mathrm{KL}}(q_\phi(\mathbf{z}|\mathbf{x})||p(\mathbf{z})), \tag{10}$$

using the reparameterisation trick to take gradients through Monte Carlo samples from $q_\phi(\mathbf{z}|\mathbf{x})$.

A.1 DISENTANGLING VAES

When learning *disentangled* representations (Bengio et al., 2013) in a VAE, one attempts to establish a one-to-one correspondence between dimensions of the learnt latent space and some interpretable aspect of the data (Higgins et al., 2017a; Burgess et al., 2017; Chen et al., 2018; Mathieu et al., 2019). One dimension of the latent space could encode the rotation of a face for instance. Mathieu et al. (2019) offers a broader perspective, where disentangling can be interpreted as a particular case of *decomposition*. In decomposition, models have the right degree of overlap between their latent posteriors such that the aggregate posterior matches the prior well throughout the latent space $\mathcal{Z}$.

Disentangling is often enforced by an added penalisation to the VAE ELBO that acts akin to a regularisation method. Because of this, disentangling can be difficult to achieve in practice, and often requires precisely choosing the hyperparameters of the model *and* of the weighting of the added regularisation term (Locatello et al., 2019; Mathieu et al., 2019; Rolinek et al., 2019). That disentangling relies on forms of soft supervision renders the task of learning disentangled representations potentially problematic (Khemakhem et al., 2020). When viewed as a purely unsupervised task it can be hard to establish a direct correspondence between a disentangling-VAE's training objective and the learning of a disentangled latent space. Nevertheless, models trained under disentangling objectives have other beneficial properties. For example, the encoders of some disentangled VAEs have been used as the perceptual part of deep reinforcement learning models to create agents more robust to variation in their environment (Higgins et al., 2017b). Thus, regardless of the presence of disentangled generative factors, these regularization methods can be useful for downstream tasks. In this paper we show that methods developed to obtain disentangled representations have the benefit of conferring robustness to adversarial attack.

A commonly used disentangling method is that of the β-VAE. In a β-VAE (Higgins et al., 2017a), a free parameter β multiplies the D_{KL} term in the evidence lower bound $\mathcal{L}(\mathbf{x})$. This objective $\mathcal{L}_\beta(\mathbf{x})$ remains a lower bound on the evidence:

$$\mathcal{L}_\beta(\mathbf{x}) := \mathbb{E}_{q_\phi(\mathbf{z}|\mathbf{x})}\left[\,\log p_\theta(\mathbf{x}|\mathbf{z})\right] - \beta D_{\mathrm{KL}}(q_\phi(\mathbf{z}|\mathbf{x})||p(\mathbf{z}))]$$

The β-VAE though it offers a simple method for obtaining potentially disentangled representations does so at the expense of model quality. Models trained with large β penalisation suffer from poor quality reconstructions and lower ELBO.

Other methods seek to offset this degradation in model quality by decomposing the ELBO and more precisely targeting the regularisation so as to lessen the degradation in model quality when obtaining disentangled representations. We can more insight into VAEs by defining the evidence lower bound not per data-point, but instead over the dataset $\mathcal{D}$ of size N, $\mathcal{D} = \{\mathbf{x}^n\}$, so we have $\mathcal{L}(\theta, \phi, \mathcal{D})$ (Hoffman & Johnson, 2016; Makhzani et al., 2016; Kim & Mnih, 2018; Chen et al., 2018; Esmaeili et al., 2019). From this, Esmaeili et al. (2019) gives a decomposition of the dataset-level evidence

lower bound:

$$\mathcal{L}(\theta, \phi, \mathcal{D}) = \mathbb{E}_{q_\phi(\mathbf{z},\mathbf{x})} \log \frac{p_\theta(\mathbf{x}, \mathbf{z})}{q_\phi(\mathbf{z}, \mathbf{x})} \tag{11}$$

$$= \mathbb{E}_{q_\phi(\mathbf{z},\mathbf{x})} \big[\underbrace{\log \frac{p_\theta(\mathbf{x}|\mathbf{z})}{p_\theta(\mathbf{x})}}_{①} - \underbrace{\log \frac{q_\phi(\mathbf{z}|\mathbf{x})}{q_\phi(\mathbf{z})}}_{②} \big] - \underbrace{D_{\mathrm{KL}}(q(\mathbf{x})||p_\theta(\mathbf{x}))}_{③} - \underbrace{D_{\mathrm{KL}}(q_\phi(\mathbf{z})||p(\mathbf{z}))}_{④} \tag{12}$$

where under the assumption that $p(\mathbf{z})$ factorises we can further decompose ④:

$$D_{\mathrm{KL}}(q_\phi(\mathbf{z})||p(\mathbf{z})) = \mathbb{E}_{q_\phi(\mathbf{z})} \underbrace{\big[\log \frac{q_\phi(\mathbf{z})}{\prod_j q_\phi(\mathbf{z}_j)} \big]}_{Ⓐ} + \sum_j \underbrace{D_{\mathrm{KL}}(q_\phi(\mathbf{z}_j)||p(\mathbf{z}_j))}_{Ⓑ} \tag{13}$$

where j indexes over coordinates in $\mathbf{z}$. $q_\phi(\mathbf{z}, \mathbf{x}) = q_\phi(\mathbf{z}|\mathbf{x})q(\mathbf{x})$ and $q(\mathbf{x}) := \frac{1}{N}\sum_{n=1}^{N} \delta(\mathbf{x} - \mathbf{x}^n)$ is the empirical data distribution. $q_\phi(\mathbf{z}) := \frac{1}{N}\sum_{n=1}^{N} q_\phi(\mathbf{z}|\mathbf{x}^n)$ is called the aggregate posterior.

Ⓐ is the total correlation (TC) for $q_\phi(\mathbf{z})$.

Definition A.1. *The total correlation (TC) is a generalisation of mutual information to multiple variables (Watanabe, 1960) and is often used as the objective Independent Component Analysis (Bell & Sejnowski, 1995). The TC is defined as is defined as the KL divergence from the joint distribution $p(\mathbf{s}), \mathbf{s} \in \mathbb{R}^d$ to the independent distribution over the dimensions of the variable $\mathbf{s}$: $p(\mathbf{s}_1)p(\mathbf{s}_2)\dots p(\mathbf{s}_n)$. Formally: $\mathrm{TC}(\mathbf{s}) = D_{\mathrm{KL}}(p(\mathbf{s})|| \prod_{j=1}^{d} p(\mathbf{s}_j))$*

With this mean-field $p(\mathbf{z})$, Factor and β-TCVAEs upweight the TC of the aggregate posterior, so we have an objective:

$$\mathcal{L}^{\beta\mathrm{TC}}(\theta, \phi, \mathcal{D}) = ① + ② + ③ + Ⓑ + \beta Ⓐ \tag{14}$$

Upweighting the penalisation associated with the TC term promotes the learning of independent latent factors, one of the key objectives of disentangling. Chen et al. (2018) show empirically that the learnt representations are disentangled. They also give a differentiable, stochastic approximation to $\mathbb{E}_{q_\phi(\mathbf{z})} \log q_\phi(\mathbf{z})$, rendering this decomposition simple to use as a training objective using stochastic gradient descent. However this is a biased estimator: it is a nested expectation, for which unbiased, finite–variance, estimators do not generally exist (Rainforth et al., 2018). Consequently, it has the unfortunate consequence of needing large batch sizes to have the desired behaviour; for small batch sizes its practical behaviour mimics that of the β-VAE (Mathieu et al., 2019).

A.2 Hierarchical VAEs

In a hierarchical VAE we have a set of L layers of $\mathbf{z}$ variables: $\vec{\mathbf{z}} = \{\mathbf{z}^i\}$. However, training DLGMs is challenging: the latent variables furthest from the data can fail to learn anything informative (Sønderby et al., 2016; Zhao et al., 2017). Due to the factorisation of $q_\phi(\vec{\mathbf{z}}|\mathbf{x})$ and $p_\theta(\mathbf{x}, \vec{\mathbf{z}})$ in a DLGM, it is possible for a single-layer VAE to train in isolation within a hierarchical model: each $p_\theta(\mathbf{z}^i|\mathbf{z}^{i+1})$ distribution can become a fixed distribution not depending on $\mathbf{z}^{i+1}$ such that each D_{KL} divergence present in the objective between corresponding $\mathbf{z}^i$ layers can still be driven to a local minima. (Zhao et al., 2017) gives a proof of this separation for the case where the model is perfectly trained, i.e. $D_{\mathrm{KL}}(q_\phi(\mathbf{z}, \mathbf{x})||p_\theta(\mathbf{x}, \mathbf{z})) = 0$.

This is the hierarchical version of the collapse of $\mathbf{z}$ units in a single-layer VAE (Burda et al., 2016), but now the collapse is over entire layers $\mathbf{z}^i$. It is part of the motivation for the Ladder VAE (Sønderby et al., 2016) and BIVA (Maaløe et al., 2019).

B TOTAL-CORRELATION DECOMPOSITION OF ELBO

Proof of Theorem 1

Here we prove that the ELBO for a hierarchical VAE with forward model as in Eq (2) and amortised variational posterior as in Eq (3) can be decomposed to reveal a total-correlation in the top-most latent variable.

Specifically, now considering the ELBO for the whole dataset and using $q(\mathbf{x})$ to indicate the empirical data distribution, we will obtain, denoting $\mathbf{z}^0 = \mathbf{x}$:

$$\begin{aligned}\mathcal{L}(\theta,\phi;\mathcal{D}) &= \mathbb{E}_{q_\phi(\vec{\mathbf{z}},\mathbf{x})}\left[\log p_\theta(\mathbf{x}|\vec{\mathbf{z}})\right] - \mathbb{E}_{q_\phi(\vec{\mathbf{z}}|\mathbf{x})q(\mathbf{x})}\left[\sum_{i=1}^{L-1} D_{\mathrm{KL}}(q_\phi(\mathbf{z}^i|\mathbf{z}^{i-1},\mathbf{x})||p_\theta(\mathbf{z}^i|\mathbf{z}^{i+1}))\right] \\ &- \mathbb{E}_{q_\phi(\mathbf{z}^{L-1})} D_{\mathrm{KL}}(q_\phi(\mathbf{z}^L,\mathbf{x}|\mathbf{z}^{L-1})||q_\phi(\mathbf{z}^L)q(\mathbf{x})) \\ &- \sum\nolimits_j D_{\mathrm{KL}}(q_\phi(\mathbf{z}_j^L)||p(\mathbf{z}_j^L)) - \beta D_{\mathrm{KL}}\Big(q_\phi(\mathbf{z}^L)||\prod\nolimits_j q_\phi(\mathbf{z}_j^L)\Big) \end{aligned} \tag{15}$$

We start with the forms of p and q given in Theorem 1. The likelihood is conditioned on all $\mathbf{z}$ layers: $p_\theta(\mathbf{x}|\vec{\mathbf{z}})$.

$$\begin{aligned}\mathcal{L}(\theta,\phi;\mathcal{D}) &= \mathbb{E}_{q_\phi(\vec{\mathbf{z}},\mathbf{x})} \log \frac{p_\theta(\mathbf{x},\vec{\mathbf{z}})}{q_\phi(\vec{\mathbf{z}},\mathbf{x})} && (16)\\ &= \mathbb{E}_{q_\phi(\vec{\mathbf{z}},\mathbf{x})}\left[\log p_\theta(\mathbf{x}|\vec{\mathbf{z}})\right] - \mathbb{E}_{q(\mathbf{x})}\left[D_{\mathrm{KL}}(q_\phi(\vec{\mathbf{z}},\mathbf{x})||p_\theta(\vec{\mathbf{z}}))\right] && (17)\\ &= \mathbb{E}_{q(\vec{\mathbf{z}},\mathbf{x})} \log p_\theta(\mathbf{x}|\vec{\mathbf{z}}) - \mathbb{E}_{q(\mathbf{x})} \log q(\mathbf{x}) + \mathbb{E}_{q(\vec{\mathbf{z}},\mathbf{x})} \log \frac{p_\theta(\vec{\mathbf{z}})}{q(\vec{\mathbf{z}}|\mathbf{x})} && (18)\\ &= \mathbb{E}_{q(\vec{\mathbf{z}},\mathbf{x})} \log p_\theta(\mathbf{x}|\vec{\mathbf{z}}) + \mathcal{H}(q(\mathbf{x})) && (19)\\ &\quad + \underbrace{\int \mathrm{d}\mathbf{x}\,\mathrm{d}\mathbf{z}^1 \prod_{i=2}^{L}(\mathrm{d}\mathbf{z}^i q_\phi(\mathbf{z}^i|\mathbf{z}^{i-1},\mathbf{x})) q_\phi(\mathbf{z}^1|\mathbf{x}) q(\mathbf{x}) \log \frac{p(\mathbf{z}^L)\prod_{k=1}^{L-1} p_\theta(\mathbf{z}^k|\mathbf{z}^{k+1})}{q_\phi(\mathbf{z}^1|\mathbf{x})\prod_{m=1}^{L-1} q_\phi(\mathbf{z}^{m+1}|\mathbf{z}^m,\mathbf{x})}}_{\text{W}} \end{aligned}$$

So here we have three terms: an expectation over the data likelihood, the entropy of the empirical data distribution (a constant) and W. We now can expand W to a term involving the prior for the latent $\mathbf{z}^L$ and a term involving the conditional distributions from the generative model for the remaining components of $\vec{\mathbf{z}}$:

$$\begin{aligned}\text{W} &= \underbrace{\int \mathrm{d}\mathbf{x} \prod_{i=1}^{L}(\mathrm{d}\mathbf{z}^i) q_\phi(\vec{\mathbf{z}}|\mathbf{x}) q(\mathbf{x}) \log \frac{\prod_{k=1}^{L-1} p_\theta(\mathbf{z}^k|\mathbf{z}^{k+1})}{q_\phi(\mathbf{z}^1|\mathbf{x})\prod_{m=1}^{L-2} q_\phi(\mathbf{z}^{m+1}|\mathbf{z}^m,\mathbf{x})}}_{\text{R}} \\ &\quad + \underbrace{\int \mathrm{d}\mathbf{x} \prod_{i=1}^{L}(\mathrm{d}\mathbf{z}^i) q_\phi(\vec{\mathbf{z}}|\mathbf{x}) q(\mathbf{x}) \log \frac{p(\mathbf{z}^L)}{q_\phi(\mathbf{z}^L|\mathbf{z}^{L-1},\mathbf{x})}}_{\text{S}} \end{aligned} \tag{20}$$

The first part R, it that part of W not involving the prior for 'top-most' latent variable $\mathbf{z}^L$, is the first subject of our attention. We split out the part of R involving the generative and posterior terms for the latent variable closest to the data, $\mathbf{z}^1$ and the rest:

$$\text{R} = \underbrace{\int \mathrm{d}\mathbf{x} \prod_{i=1}^{L}(\mathrm{d}\mathbf{z}^i) q_\phi(\vec{\mathbf{z}}|\mathbf{x}) q(\mathbf{x}) \log \frac{p_\theta(\mathbf{z}^1|\mathbf{z}^2)}{q_\phi(\mathbf{z}^1|\mathbf{x})}}_{\text{R}_a} + \underbrace{\sum_{m=2}^{L-1} \int \mathrm{d}\mathbf{x} \prod_{i=1}^{L}(\mathrm{d}\mathbf{z}^i) q_\phi(\vec{\mathbf{z}}|\mathbf{x}) q(\mathbf{x}) \log \frac{p_\theta(\mathbf{z}^m|\mathbf{z}^{m+1})}{q_\phi(\mathbf{z}^m|\mathbf{z}^{m-1},\mathbf{x})}}_{\text{R}_b}.$$

The first of these terms R_a is an expectation over a D_{KL}:

$$\text{R}_a = -\mathbb{E}_{q_\phi(\mathbf{z}^2,\mathbf{x})} D_{\mathrm{KL}}(q_\phi(\mathbf{z}^1|\mathbf{x})||p_\theta(\mathbf{z}^1|\mathbf{z}^2)). \tag{21}$$

And the rest, R_b, provides the D_{KL} divergences in the ELBO for all latent variables other than $\mathbf{z}^L$ and $\mathbf{z}^1$. It reduces to a sum of expectations over D_{KL} divergences, one per latent variable.

$$\text{R}_b = \sum_{m=2}^{L-1} \int \mathrm{d}\mathbf{x} \prod_{i=1}^{L} (\mathrm{d}\mathbf{z}^i) q_\phi(\mathbf{z}^1|\mathbf{x}) q(\mathbf{x}) \prod_{k=1,\neq m}^{L-1} (q_\phi(\mathbf{z}^{k+1}|\mathbf{z}^k, \mathbf{x})) q_\phi(\mathbf{z}^m|\mathbf{z}^{m-1}, \mathbf{x}) \log \frac{p_\theta(\mathbf{z}^m|\mathbf{z}^{m+1})}{q_\phi(\mathbf{z}^m|\mathbf{z}^{m-1}, \mathbf{x})} \tag{22}$$

$$= - \sum_{m=2}^{L-1} \int \mathrm{d}\mathbf{x} \prod_{i=1}^{L} (\mathrm{d}\mathbf{z}^i) q_\phi(\mathbf{z}^1|\mathbf{x}) q(\mathbf{x}) \prod_{k=1,\neq m}^{L-1} (q_\phi(\mathbf{z}^{k+1}|\mathbf{z}^k, \mathbf{x})) D_{\mathrm{KL}}(q_\phi(\mathbf{z}^m|\mathbf{z}^{m-1}, \mathbf{x}) || p_\theta(\mathbf{z}^m|\mathbf{z}^{m+1})) \tag{23}$$

$$= - \sum_{m=2}^{L-1} \mathbb{E}_{q_\phi(\mathbf{z}^{m+1}, \mathbf{z}^{m-1}, \mathbf{x})} D_{\mathrm{KL}}(q_\phi(\mathbf{z}^m|\mathbf{z}^{m-1}, \mathbf{x}) || p_\theta(\mathbf{z}^m|\mathbf{z}^{m+1})). \tag{24}$$

Now we have:

$$\mathcal{L}(\theta, \phi; \mathcal{D}) = \mathbb{E}_{q(\vec{\mathbf{z}}, \mathbf{x})} \log p_\theta(\mathbf{x}|\vec{\mathbf{z}}) + \mathcal{H}(q(\mathbf{x})) + \text{R}_a + \text{R}_b + \text{S} \tag{25}$$

We wish to apply TC decomposition to the top-most latent variable $\mathbf{z}^L$. S is an expectation over the D_{KL} divergence between $q_\phi(\mathbf{z}^L|\mathbf{z}^{L-1}, \mathbf{x})$ and $p(\mathbf{z}^L)$

$$\text{S} = - \mathbb{E}_{q_\phi(\mathbf{z}^{L-1}, \mathbf{x})} D_{\mathrm{KL}}(q_\phi(\mathbf{z}^L|\mathbf{z}^{L-1}, \mathbf{x}) || p(\mathbf{z}^L)) \tag{26}$$

Applying the decomposition, with j indexes over units in $\mathbf{z}^L$.

$$\begin{aligned}
\text{S} = &- \mathbb{E}_{q_\phi(\mathbf{z}^L, \mathbf{z}^{L-1}, \mathbf{x})} \big[\log q_\phi(\mathbf{z}^L|\mathbf{z}^{L-1}, \mathbf{x}) - \log p(\mathbf{z}^L) + \log q_\phi(\mathbf{z}^L) \\
&\qquad - \log q_\phi(\mathbf{z}^L) + \log \prod_j q_\phi(\mathbf{z}_j^L) - \log \prod_j q_\phi(\mathbf{z}_j^L) \big] \\
= &- \mathbb{E}_{q_\phi(\mathbf{z}^L, \mathbf{z}^{L-1}, \mathbf{x})} \left[\log \frac{q_\phi(\mathbf{z}^L|\mathbf{z}^{L-1}, \mathbf{x})}{q_\phi(\mathbf{z}^L)} \right] - \mathbb{E}_{q_\phi(\mathbf{z}^L)} \left[\log \frac{q_\phi(\mathbf{z}^L)}{\prod_j q_\phi(\mathbf{z}_j^L)} \right] \\
&- \mathbb{E}_{q_\phi(\mathbf{z}^L)} \left[\log \frac{\prod_j q_\phi(\mathbf{z}_j^L)}{p(\mathbf{z}^L)} \right] \\
= &- \mathbb{E}_{q_\phi(\mathbf{z}^L, \mathbf{z}^{L-1}, \mathbf{x})} \left[\log \frac{q_\phi(\mathbf{z}^L|\mathbf{z}^{L-1}) q(\mathbf{x})}{q_\phi(\mathbf{z}^L) q(\mathbf{x})} \right] - \mathbb{E}_{q_\phi(\mathbf{z}^L)} \left[\log \frac{q_\phi(\mathbf{z}^L)}{\prod_j q_\phi(\mathbf{z}_j^L)} \right] \\
&- \sum_j \mathbb{E}_{q_\phi(\mathbf{z}^L)} \left[\log \frac{q_\phi(\mathbf{z}_j^L)}{p(\mathbf{z}_j^L)} \right] \\
= &\underbrace{- \mathbb{E}_{q_\phi(\mathbf{z}^{L-1})}) D_{\mathrm{KL}}(q_\phi(\mathbf{z}^L, \mathbf{x}|\mathbf{z}^{L-1}) || q_\phi(\mathbf{z}^L) q(\mathbf{x}))}_{\text{S}_a} \\
&\underbrace{- \sum_j D_{\mathrm{KL}}(q_\phi(\mathbf{z}_j^L) || p(\mathbf{z}_j^L))}_{\text{S}_b} \underbrace{- D_{\mathrm{KL}}(q_\phi(\mathbf{z}^L) || \prod_j q_\phi(\mathbf{z}_j^L))}_{\text{S}_c}
\end{aligned}$$

Where we have used $p(\mathbf{z}^L) = \prod_j p(\mathbf{z}_j^L)$ for our chosen generative model, a product of independent unit-variance Gaussian distributions.

$$\mathcal{L}(\theta, \phi; \mathcal{D}) = \mathbb{E}_{q(\vec{\mathbf{z}}, \mathbf{x})} \log p_\theta(\mathbf{x}|\vec{\mathbf{z}}) + \mathcal{H}(q(\mathbf{x})) + \text{R}_a + \text{R}_b + \text{S}_a + \text{S}_b + \text{S}_c \tag{27}$$

Giving us a decomposition of the evidence lower bound that reveals the TC-term in $\mathbf{z}^L$, as required. Multiplying this with a chosen prefactor β gives us the required form. □

C MINIBATCH WEIGHTED SAMPLING

As in Chen et al. (2018), applying β-TC decomposition requires us to calculate terms of the form:

$$\mathbb{E}_{q_\phi(\mathbf{z}^i)} \log q_\phi(\mathbf{z}^i) \tag{28}$$

The $i = 1$ case is covered in the appendix of Chen et al. (2018). First we will repeat the argument for $i = 1$ as made in Chen et al. (2018), but in our notation, and then we cover the case $i > 1$ for models with factorisation of $q_\phi(\vec{\mathbf{z}}|\mathbf{x})$ of Seatbelt VAEs.

C.1 MWS FOR β-TCVAES

We denote $\mathcal{B}_M = \{\mathbf{x}_1, \mathbf{x}_2, ..., \mathbf{x}_M\}$, a minibatch of datapoints drawn uniformly iid from $q(\mathbf{x}) = 1/N \sum_{n=1}^{N} \delta(\mathbf{x} - \mathbf{x}_n)$. For any minibatch we have $p(\mathcal{B}_M) = \frac{1}{N}^M$. Chen et al. (2018) introduce $r(\mathcal{B}_M|\mathbf{x})$, the probability of a sampled minibatch given that one member is x and the remaining $M - 1$ points are sampled iid from $q(\mathbf{x})$, so $r(\mathcal{B}_M|\mathbf{x}) = \frac{1}{N}^{M-1}$.

$$\begin{aligned}
\mathbb{E}_{q_\phi(\mathbf{z}^1)} \log q_\phi(\mathbf{z}^1) &= \mathbb{E}_{q_\phi(\mathbf{z}^1,\mathbf{x})} \left[\log \mathbb{E}_{q(\mathbf{x})} \left[q_\phi(\mathbf{z}^1|\mathbf{x}) \right] \right] && (29)\\
&= \mathbb{E}_{q_\phi(\mathbf{z}^1,\mathbf{x})} \left[\log \mathbb{E}_{p(\mathcal{B}_M)} \left[\frac{1}{M} \sum_{m=1}^{M} q_\phi(\mathbf{z}^1|\mathbf{x}_m) \right] \right] && (30)\\
&\geq \mathbb{E}_{q_\phi(\mathbf{z}^1,\mathbf{x})} \left[\log \mathbb{E}_{r(\mathcal{B}_M|\mathbf{x})} \left[\frac{p(\mathcal{B}_M)}{r(\mathcal{B}_M|\mathbf{x})} \frac{1}{M} \sum_{m=1}^{M} q_\phi(\mathbf{z}^1|\mathbf{x}_m) \right] \right] && (31)\\
&= \mathbb{E}_{q_\phi(\mathbf{z}^1,\mathbf{x})} \left[\log \mathbb{E}_{r(\mathcal{B}_M|\mathbf{x})} \left[\frac{1}{NM} \sum_{m=1}^{M} q_\phi(\mathbf{z}^1|\mathbf{x}_m) \right] \right] && (32)\\
& && (33)
\end{aligned}$$

So then during training, one samples a minibatch $\{\mathbf{x}_1, \mathbf{x}_2, ..., \mathbf{x}_M\}$ and can estimate $\mathbb{E}_{q_\phi(\mathbf{z}^1)} \log q_\phi(\mathbf{z}^1)$ as:

$$\mathbb{E}_{q_\phi(\mathbf{z}^1)} \log q_\phi(\mathbf{z}^1) \approx \frac{1}{M} \sum_{i=1}^{M} \left[\log \sum_{j=1}^{M} q_\phi(\mathbf{z}_i^1|\mathbf{x}_j) - \log NM \right] \tag{34}$$

and $\mathbf{z}_i^1$ is a sample from $q_\phi(\mathbf{z}^1|\mathbf{x}_i)$.

C.2 MINIBATCH WEIGHTED SAMPLING FOR SEATBELT-VAES

Here we have that $q(\vec{\mathbf{z}}, \mathbf{x}) = \prod_{l=2}^{L} [q_\phi(\mathbf{z}^l|\mathbf{z}^{l-1}, \mathbf{x})] q_\phi(\mathbf{z}^1|\mathbf{x}) q(\mathbf{x})$. Now instead of having a minibatch of datapoints, we have a minibatch of draws of $\mathbf{z}^{i-1}$: $\mathcal{B}_M^{i-1} = \{\mathbf{z}_1^{i-1}, \mathbf{z}_2^{i-1}, ..., \mathbf{z}_M^{i-1}\}$. Each member of which is the result of sequentially sampling along a chain, starting with some particular datapoint $\mathbf{x}_m \sim q(\mathbf{x})$.

For $i > 2$, members of $\mathcal{B}_M^{i-1}$ are drawn:

$$\mathbf{z}_j^{i-1} \sim q_\phi(\mathbf{z}^{i-1}|\mathbf{z}_j^{i-2}, \mathbf{x}_j) \tag{35}$$

and for $i = 2$:

$$\mathbf{z}_j^1 \sim q_\phi(\mathbf{z}^1|\mathbf{x}_j) \tag{36}$$

Thus each member of this batch $\mathcal{B}_M^{i-1}$ is the descendant of a particular datapoint that was sampled in an iid minibatch $\mathcal{B}_M$ as defined above. We similarly define $r(\mathcal{B}_M^{i-1}|\mathbf{z}^{i-1}, \mathbf{x})$ as the probability of selecting a particular minibatch $\mathcal{B}_M^{i-1}$ of these values out from our set $\{(\mathbf{x}_n, \mathbf{z}_n^{i-1})\}$ (of cardinality N) given that we have selected into our minibatch one particular pair of values $(\mathbf{x}, \mathbf{z}^{i-1})$ from these N values. Like above, $r(\mathcal{B}_M^{i-1}|\mathbf{z}^{i-1}, \mathbf{x}) = \frac{1}{N}^{M-1}$

Now we can consider $\mathbb{E}_{q_\phi(\mathbf{z}^i)} \log q_\phi(\mathbf{z}^i)$ for $i > 1$:

$$\mathbb{E}_{q_\phi(\mathbf{z}^i)} \log q_\phi(\mathbf{z}^i) = \mathbb{E}_{q_\phi(\mathbf{z}^i, \mathbf{z}^{i-1}, \mathbf{x})} [\log \mathbb{E}_{q_\phi(\mathbf{z}^{i-1}, \mathbf{x})} [q_\phi(\mathbf{z}^i | \mathbf{z}^{i-1}, \mathbf{x})]] \tag{37}$$

$$= \mathbb{E}_{q_\phi(\mathbf{z}^i, \mathbf{z}^{i-1}, \mathbf{x})} [\log \mathbb{E}_{p(\mathcal{B}_M^{i-1})} [\frac{1}{M} \sum_{m=1}^{M} q_\phi(\mathbf{z}^i | \mathbf{z}_m^{i-1}, \mathbf{x}_m)]] \tag{38}$$

$$\geq \mathbb{E}_{q_\phi(\mathbf{z}^i, \mathbf{z}^{i-1}, \mathbf{x})} [\log \mathbb{E}_{r(\mathcal{B}_M^{i-1} | \mathbf{z}^{i-1}, \mathbf{x})} [\frac{p(\mathcal{B}_M^{i-1})}{r(\mathcal{B}_M^{i-1} | \mathbf{z}^{i-1}, \mathbf{x})} \frac{1}{M} \sum_{m=1}^{M} q_\phi(\mathbf{z}^i | \mathbf{z}_m^{i-1}, \mathbf{x}_m)]] \tag{39}$$

$$= \mathbb{E}_{q_\phi(\mathbf{z}^i, \mathbf{z}^{i-1}, \mathbf{x})} [\log \mathbb{E}_{r(\mathcal{B}_M^{i-1} | \mathbf{z}^{i-1}, \mathbf{x})} [\frac{1}{NM} \sum_{m=1}^{M} q_\phi(\mathbf{z}^i | \mathbf{z}_m^{i-1}, \mathbf{x}_m)]] \tag{40}$$

Where we have followed the same steps as in the previous subsection.

During training, one samples a minibatch $\{\mathbf{z}_1^{i-1}, \mathbf{z}_2^{i-1}, ..., \mathbf{z}_M^{i-1}\}$, where each is constructed by sampling ancestrally. Then one can estimate $\mathbb{E}_{q_\phi(\mathbf{z}^i)} \log q_\phi(\mathbf{z}^i)$ as:

$$\mathbb{E}_{q_\phi(\mathbf{z}^i)} \log q_\phi(\mathbf{z}^i) \approx \frac{1}{M} \sum_{k=1}^{M} [\log \sum_{j=1}^{M} q_\phi(\mathbf{z}_k^i | \mathbf{z}_j^{i-1}, \mathbf{x}_j) - \log NM] \tag{41}$$

and $\mathbf{z}_k^i$ is a sample from $q_\phi(\mathbf{z}^i | \mathbf{z}_k^{i-1}, \mathbf{x}_k)$. In our approach we only need terms of this form for $i = L$, so we have:

$$\mathbb{E}_{q_\phi(\mathbf{z}^L)} \log q_\phi(\mathbf{z}^L) \approx \frac{1}{M} \sum_{k=1}^{M} [\log \sum_{j=1}^{M} q_\phi(\mathbf{z}_k^L | \mathbf{z}_j^{L-1}, \mathbf{x}_j) - \log NM] \tag{42}$$

and $\mathbf{z}_k^L$ is a sample from $q_\phi(\mathbf{z}^L | \mathbf{z}_k^{L-1}, \mathbf{x}_k)$.

D SEATBELT-VAE RESULTS

D.1 SEATBELT-VAE LAYERWISE ATTACKS

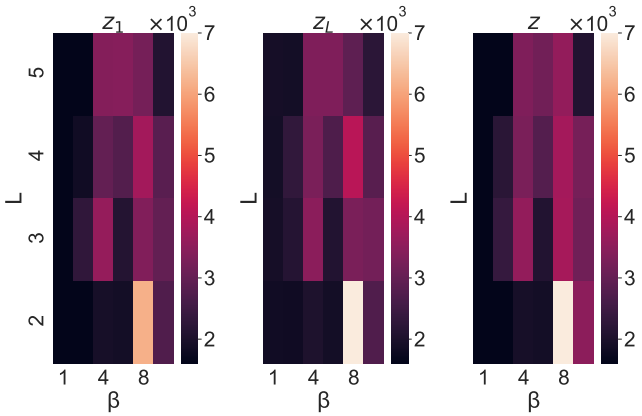

(a) 3D Faces

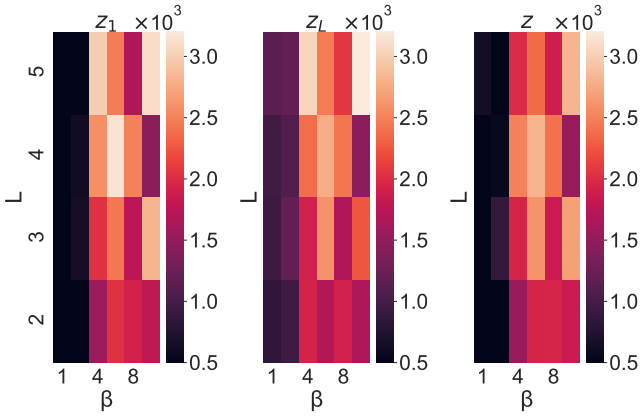

(b) Chairs

Figure D.7: $-\log p_\theta(\mathbf{x}^t|\tilde{\mathbf{z}})$, $\tilde{z} \sim q(\mathbf{z}|\mathbf{x}+d)$ where d is some adversarial distortion, for Seatbelt-VAEs trained on (a) 3D Faces and (b) Chairs; over β and L values for *latent* attacks. We attack the bottom layer ($\mathbf{z}^1$), the top layer ($\mathbf{z}^L$), and finally show the effect when attacking all layers ($\mathbf{z}$). Larger values of $-\log p_\theta(\mathbf{x}^t|\tilde{\mathbf{z}})$ correspond to less successful adversarial attacks. Generally attacking all layers seems to give the attacker a slight advantage (as seen by the slightly lower $-\log p_\theta(\mathbf{x}^t|\tilde{\mathbf{z}})$ values for Faces and Chairs).

D.2 SEATBELT-VAE ATTACKS BY MODEL DEPTH AND β

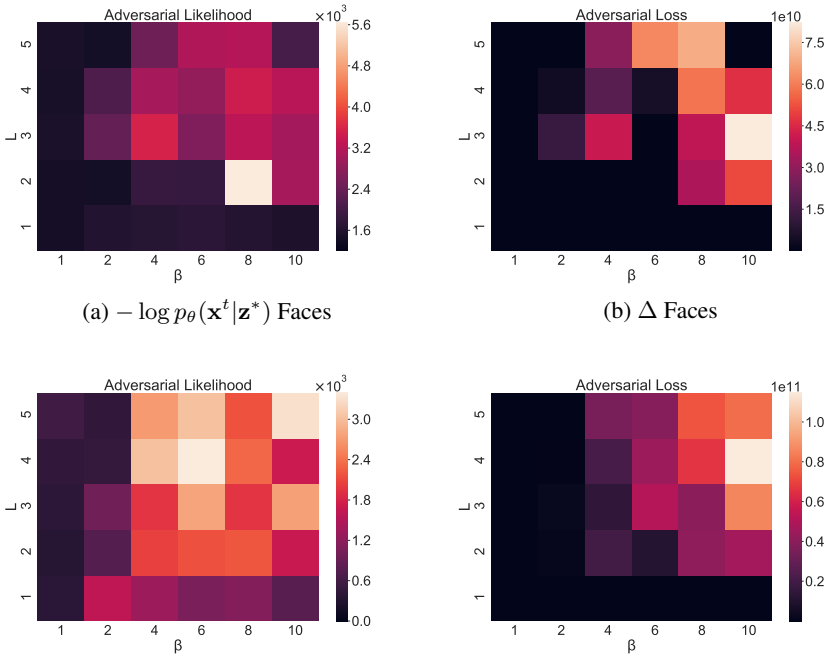

(a) $-\log p_\theta(\mathbf{x}^t|\mathbf{z}^*)$ Faces

(b) Δ Faces

(c) $-\log p_\theta(\mathbf{x}^t|\mathbf{z}^*)$ Chairs

(d) Δ Chairs

Figure D.8: Here we measure the robustness of TC-penalised models numerically. Sub-figures (a) and (c) show $-\log p_\theta(\mathbf{x}^t|\mathbf{z}^*)$, the adversarial likelihood of a target image $\mathbf{x}^t$ given an attacked latent representation $\mathbf{z}^*$ for Seatbelt-VAEs for Chairs and 3D Faces. Larger likelihood values correspond to less successful adversarial attacks. Sub-figures (b) and (d) show adversarial loss Δ for Seatbelt-VAEs for Chairs and 3D Faces. We show these likelihood and loss values over β and L (total number of stochastic layers) values for attacks. Note that the bottom rows of all figures have $L = 1$, and thus correspond to β-TCVAEs. The leftmost column corresponds to models with $\beta = 1$, which are vanilla VAEs and hierarchical VAEs. As we go to the largest values of β and L for both Chairs and 3D Faces, Δ grows by a factor of $\approx 10^7$ and $-\log p_\theta(\mathbf{x}^t|\mathbf{z}^*)$ doubles. These results tell us that depth and TC-penalisation together, i.e Seatbelt-VAE, can offer immense protection from the adversarial attacks studied.

E AGGREGATE ANALYSIS OF ADVERSARIAL ATTACK

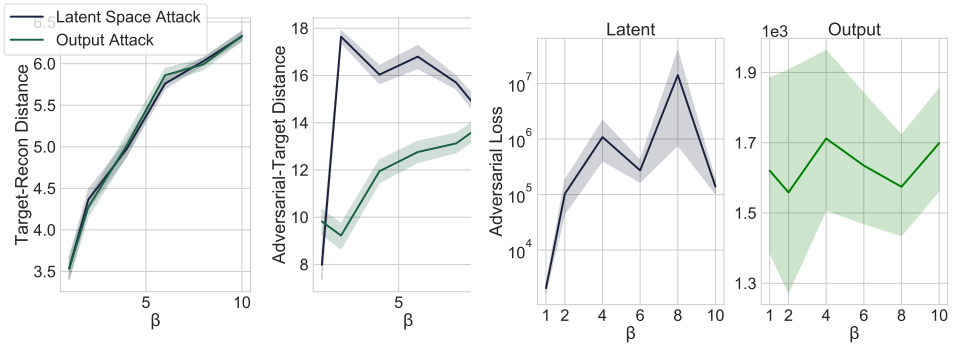

(a) dSprites Distances (b) dSprites Losses

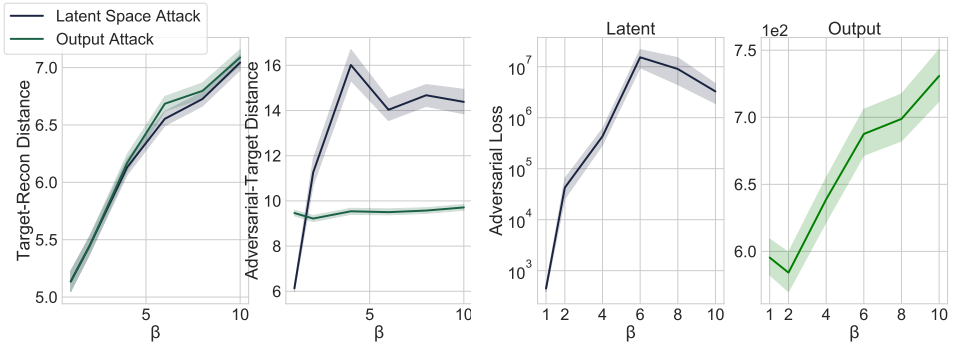

(c) Chairs Distances (d) Chairs Losses

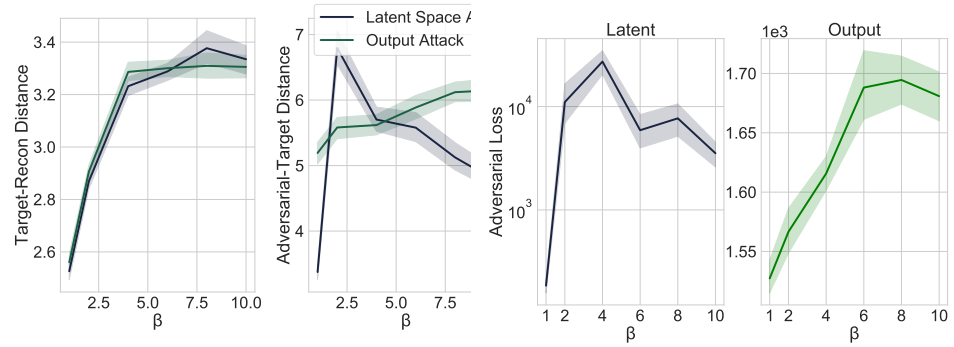

(e) 3D Faces Distances (f) 3D Faces Losses

Figure E.9: Plots showing the effect of varying β in a β-TCVAE trained on dSprites (a,b), Chairs (c,d), and 3D Faces (d,e) on: the L_2 distance from the adversarial target x^t to its reconstruction when given as input (target-recon distance) and the L_2 distance between the adversarial input x^* and x^t (adversarial-target distance); and the adversarial objectives Δ. We also include these metrics for "output" attacks Gondim-Ribeiro et al. (2018), which we find to be generally less effective. In such attacks the attacker directly tries to reduce the L2 distance between the reconstructed output and the target image. For latent attacks the adversarial-target L_2 distance grows more rapidly than the target-recon distance (i.e the degradation of reconstruction quality) as we increase β. This effect is much less clear for output attacks. This makes it apparent that the robustness we see in β-TCVAE to latent space adversarial attacks is not due the degradation in reconstruction quality we see as β increases. It is also apparent that increasing β increases the adversarial loss for latent attacks and output attacks.

F ROBUSTNESS TO NOISE

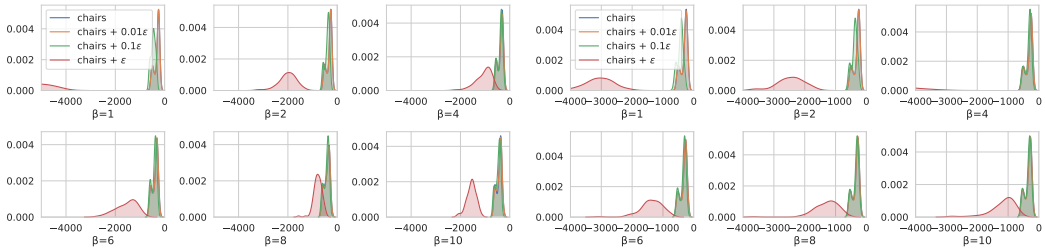

(a) Chairs β-TCVAE $\log p_\theta(\mathbf{x}|\mathbf{z})$

(b) Chairs Seatbelt-VAE $\log p_\theta(\mathbf{x}|\mathbf{z})$

Figure F.10: Here we measure the robustness of both β-TCVAE and Seatbelt-VAE when Gaussian noise is added to Chairs. Within each plot a range of β values are shown. We evaluate each model's ability to decode a noisy embedding to the original non-noised data $\mathbf{x}$ by measuring the distribution of $\log p_\theta(\mathbf{x}|\mathbf{z})$ when $\mathbf{z} \sim q_\phi(\mathbf{z}|\mathbf{x} + a\boldsymbol{\epsilon})$ (a some scaling factor taking values in $\{0.1, 0.5, 1\}$ and $\epsilon \sim \mathcal{N}(0, 1)$) for which higher values indicate better denoising. We show these likelihood values as density plots for the β-TCVAE in (a) and for the Seatbelt-VAE with $L = 4$ in (b), taking $\beta \in \{1, 2, 4, 6, 8, 10\}$. Note the axis scalings are different for each subplot. We see that for both models using $\beta > 1$ produces autoencoders that are better at denoising their inputs. Namely, the mean of the density, i.e. $\mathbb{E}_{q_\phi(\mathbf{z}|\mathbf{x}+\boldsymbol{\epsilon})}[\log p_\theta(\mathbf{x}|\mathbf{z})]$, shifts dramatically to higher values for $\beta > 1$ relative to $\beta = 1$. In other words, for both these models, the likelihood of the dataset in the noisy setting is much closer to the non-noisy dataset when $\beta > 1$ across all noise scales (0.1ϵ, 0.5ϵ, ϵ).

G IMPLEMENTATION DETAILS

All runs were done on the Azure cloud system on NC6 GPU machines.

G.1 ENCODER AND DECODER ARCHITECTURES

We used the same convolutional network architectures as Chen et al. (2018). For the encoders of all our models ($q(\cdot|\mathbf{x})$) we used purely convolutional networks with 5 convolutional layers. When training on single-channel (binary/greyscale) datasets such as dSprites, 3D Faces, or Chairs the 5 layers took the following number of filters in order: $\{32, 32, 64, 64, 512\}$. For more complex RGB datasets, such as CelebA, the layers had the following number of filters in order: $\{64, 64, 128, 128, 512\}$. The mean and variance of the amortised posteriors are the output of dense layers acting on the output of the purely convolutional network, where the number of neurons in these layers is equal to the dimensionality of the latent space $\mathcal{Z}$.

Similarly, for the decoders ($p(\mathbf{x}|\mathbf{z})$) of all our models we also used purely convolutional networks with 6 deconvolutional layers. When training on single-channel (binary/greyscale) datasets, dSprites, 3D Faces, or Chairs, the 6 layers took the following number of filters in order: $\{512, 64, 64, 32, 32, 1\}$. For CelebA the layers had the following number of filters in order: $\{512, 128, 128, 64, 64, 3\}$. The mean of the likelihood $p(\mathbf{x}|\cdot)$ was directly encoded by the final de-convolutional layer. The variance of the decoder, σ, was fixed to 0.1.

For β-TCVAE the range of $d_{\mathbf{z}}$ values used was $\{4, 6, 8, 16, 32, 64, 128\}$. For Seatbelt-VAEs the number of units in each layer $\mathbf{z}^i$ decreases sequentially. There is a list $\mathrm{z_sizes}$ for each dataset, and for a model of L layers that the last L entries to give $d_{\mathbf{z},i}, i \in \{1, ..., L\}$.

$$\{d_{\mathbf{z}}\}^{\mathrm{dSprites}} = \{96, 48, 24, 12, 6\} \tag{43}$$

$$\{d_{\mathbf{z}}\}^{\mathrm{Chairs}} = \{96, 48, 24, 12, 6\} \tag{44}$$

$$\{d_{\mathbf{z}}\}^{\mathrm{3DFaces}} = \{96, 48, 24, 12, 6\} \tag{45}$$

$$\{d_{\mathbf{z}}\}^{\mathrm{CelebA}} = \{256, 128, 64, 32\} \tag{46}$$

For Seatbelt-VAEs we also have the mappings $q_\phi(\mathbf{z}^{i+1}|\mathbf{z}^i, \mathbf{x})$ and $p_\theta(\mathbf{z}^i|\mathbf{z}^{i+1})$. These are amortised as MLPs with 2 hidden layers with batchnorm and Leaky-ReLU activation. The dimensionality of the hidden layers also decreases as a function of layer index i:

$$d_{\mathbf{h}}(q_\phi(\mathbf{z}^{i+1}|\mathbf{z}^i, \mathbf{x})) = \mathrm{h}_{\mathrm{sizes}}[i] \tag{47}$$

$$d_{\mathbf{h}}(p_\theta(\mathbf{z}^i|\mathbf{z}^{i+1})) = \mathrm{h}_{\mathrm{sizes}}[i] \tag{48}$$

$$\mathrm{h}_{\mathrm{sizes}} = [1024, 512, 256, 128, 64] \tag{49}$$

To train the model we used ADAM Kingma & Lei Ba (2015) with default parameters, a cosine decaying learning rate of 0.001, and a batch size of 1024. All data was preprocessed to fall on the interval -1 to 1. CelebA and Chairs were both downsampled and cropped as in Chen et al. (2018) and Kulkarni et al. (2015) respectively. We find that using *free-bits* regularisation Kingma et al. (2016) greatly ameliorates the optimisation challenges associated with DLGMs.